Computational Challenges in Simulating and Analyzing Experimental Linear and Nonlinear Circular Dichroism Spectra. R-(+)-1,1 '-Bis(2-naphthol) as a Prototype Case

ARTICLE *in* THE JOURNAL OF PHYSICAL CHEMISTRY B · FEBRUARY 2011

Impact Factor: 3.3 · DOI: 10.1021/jp108669f · Source: PubMed

7 AUTHORS, INCLUDING:

Fabrizio Santoro
Italian National Research Council
141 PUBLICATIONS **2,870** CITATIONS
SEE PROFILE

Xian Zhao
Shandong University
227 PUBLICATIONS **1,959** CITATIONS
SEE PROFILE

Leonardo De Boni
University of São Paulo
103 PUBLICATIONS **1,126** CITATIONS
SEE PROFILE

Antonio Rizzo
Italian National Research Council
338 PUBLICATIONS **3,056** CITATIONS
SEE PROFILE

THE JOURNAL OF PHYSICAL CHEMISTRY B

ARTICLE

pubs.acs.org/JPCB

Computational Challenges in Simulating and Analyzing Experimental Linear and Nonlinear Circular Dichroism Spectra. *R*-(+)-1,1′-Bis(2-naphthol) as a Prototype Case

Na Lin,[†,‡] Fabrizio Santoro,[§,▽] Xian Zhao,[†] Carlos Toro,[∥] Leonardo De Boni,[∥] Florencio E. Hernández,[∥,⊥] and Antonio Rizzo[*,#]

[†]State Key Laboratory of Crystal Materials, Shandong University, 250100 Jinan, Shandong, People's Republic of China

[‡]Centre for Theoretical and Computational Chemistry, Department of Chemistry, University of Tromsø, N-9037 Tromsø, Norway

[§]CNR - Consiglio Nazionale delle Ricerche, Istituto dei Composti Organometallici (ICCOM-CNR), UoS di Pisa, Area della Ricerca, Via G. Moruzzi 1, I-56124 Pisa, Italy

[∥]Department of Chemistry, University of Central Florida, P.O. Box 162366, Orlando, Florida 382616-2366, United States

[⊥]The College of Optics and Photonics, CREOL University of Central Florida, P.O. Box 162366, Orlando, Florida 382616-2366, United States

[#]CNR - Consiglio Nazionale delle Ricerche, Istituto per i Processi Chimico Fisici (IPCF-CNR), UoS di Pisa, Area della Ricerca, Via G. Moruzzi 1, I-56124 Pisa, Italy

Supporting Information

ABSTRACT: One- and two-photon circular dichroism spectra of *R*-(+)-1,1′-bis(2-naphthol), BINOL, a prototype system showing structural chirality, were calculated, in both the gas and solvated phases, in a region of wavelengths extending down to 200 nm, by applying the time-dependent density functional theory response theory. Here we emphasize the computational challenges of such a simulation. The effect of the choice of the exchange−correlation functional is carefully analyzed. We compare results obtained, with correlation-consistent basis sets of double-ζ quality, with both the popular Becke's three-parameter exchange, Lee, Yang, and Parr correlation (B3LYP) functional, and the Coulomb attenuating method based on B3LYP (CAM-B3LYP) functional. For a better analysis of the reliability of the computational model, also one- and two-photon absorption spectra are calculated. Two-photon absorption and dichroism spectra of BINOL have been measured in our group recently. Experimental features are characterized in terms of molecular excitations and the differences in the response of each state in the one- and two-photon processes are highlighted. We analyze and discuss the possible causes for the theory−experiment discrepancy in intensity of the two-photon absorption and circular dichroism response. Conformational effects, which are mostly related to the rotation of the two naphthyl moieties, and/or the coupling of excitonic and charge-transfer excitations, are investigated as possible causes of enhancements of the signal.

1. INTRODUCTION

Circular dichroism,[1,2] CD, is the difference in absorption between left (LCP) and right (RCP) circularly polarized radiation by matter. This phenomenon is strictly related to chirality and it is widely used to assign molecular absolute configurations, since two enantiomers yield mirror-image CD spectra. A special role in this area is taken, particularly, by electronic circular dichroism (ECD),[3,4] the dichroic counterpart of one-photon absorption (OPA). In a chiral molecule ECD is related through a Kramers−Kronig transform,[5] to the natural optical rotation dispersion (ORD). The latter arises from the difference in refractive indices for LCP and RCP light. ECD and ORD have been often used to characterize chiral species in gas and condensed phases as well as at interfaces.[1] However, the linear nature of these effects limits their use in the short UV region in highly absorbing and scattering biological systems. Furthermore, there are cases in which the excited states are if not completely,[6] at least highly, electric dipole inactive for one-photon absorption as a consequence of their symmetry. The molecule under study here is such an example (vide infra). Other examples are given by recently synthesized alleno-acetylene macrocycles that belong to the D_4 symmetry point group and that show remarkably intense chiroptical response.[7]

The chiroptical response of highly excited electronic states inactive in OPA can be studied by exploiting a nonlinear circular spectroscopic technique called two-photon circular dichroism (TPCD).[8] TPCD, the polarization dependent two-photon process analogous of ECD, combines the 3D confocality, reduced frequency and scattering, and enhanced penetration depth of two-photon absorption (TPA) with circular dichroism.[9] Therefore, with the fingerprinting capabilities of ECD, and yet having the potential to become a useful spectroscopic alternative to

Received: September 11, 2010
Revised: November 6, 2010
Published: January 5, 2011

study chiral systems, TPCD complements the linear CD technique, by revealing the response of excited states that cannot often be characterized by linear spectroscopy. Both theoretical and experimental advancements in the field on nonlinear circular dichroism are therefore likely to provide new opportunities in the recognition and understanding of the behavior of optically active systems.

Introduced theoretically in 1975 by Tinoco[8] (see also the work of Power[10]), TPCD has seen a great revival of interest rather recently, thanks to the development of viable computational approaches.[11−15] However, experimental verification has proven to be rather challenging. Nevertheless, recently some of us developed the double L-scan technique that permits the experimental detection of well resolved TPCD and two-photon linear-circular dichroism (TPCLD) spectra for chiral samples in solution.[16] The latter measures the difference between circularly and linearly polarized TPA.[17] The novel experimental technique allowed us to measure TPCD spectra of both *S*-(−)-1,1′-bis(2-naphthol) and *R*-(+)-1,1′-bis(2-naphthol) (hereafter labeled S-BINOL and R-BINOL, respectively) in an enantiomeric ratio *S*:*R* ≥ 99:1 and *R*:*S* ≥ 99:1, respectively, in solutions of tetrahydrofuran (THF).[18,16] In addition, the independent measurements of the LCP and RCP TPA absorption spectra yielded precise information on the TPCLD. An account of the comparison between experiments and a preliminary computational analysis of TPCD has been given in ref 18 whereas in ref 19 we have presented the related study of TPCLD[17] on the same binaphthol derivatives.

1,1′-Binaphthyls are quite popular molecules in studies related to chirality. The 2,2′-substituted species in particular form quite stable enantiomers due to hindered rotation. They can be regarded as prototype molecules for the study of structural chirality, intended as chiral response not related to the existence of a chiral center but due to molecular secondary structure. This phenomenon is of primary interest for instance in biomolecules as nucleic acids and proteins (where, however, also chiral centers exist) and in molecules relevant for the synthesis of advanced materials, such as helicenes and the recently synthesized allenoacetylene oligomers. These systems show among the strongest enhancement of chiroptical properties due to secondary structure.[14,20,7]

The vibrational circular dichroism[21] and vibrational Raman optical activity[22] spectra of few 1,1′-binaphthyl derivatives, including the 2,2′-dihydroxy derivative studied here, have also been reported. While the former have been studied both experimentally and theoretically,[23,24] the latter have only been studied theoretically.[25] The UV absorption and circular dichroism spectra of these molecules have been the subject of quite a few studies.[26−29] In some cases, these studies focused on the consequences of adopting coupled dipoles or exciton mechanism[30−32,27] to explain the features and conformational dependence of their response to electromagnetic radiation in terms of excitations localized on two well separated individual chromophores.

Thanks to the recent developments in the experimental set up for TPCD measurements, it can be foreseen that this technique will find wide application in the characterization of chiral systems and, among them, of those exhibiting chiral response due to secondary structure. Therefore, and with the aim of highlighting the computational challenges that must be faced to get reliable simulations of TPCD spectra in extended systems, herein we report on the results of an extended computational study and analysis of the experimental TPCD spectra in BINOL. In fact, we expand and discuss in greater detail the results already partially reported in refs 18 and 19, which were mainly focused on the study of the experimental aspect of TPCD.

To face the challenges, and to control the reliability of our computational protocols for R-BINOL, in this paper we choose the time dependent density functional response theory (TD-DFT),[33,34] and analyze in detail, besides TPCD, ECD and the OPA and TPA spectroscopic responses, for which a wider computational experience is available. We adopt both the very popular Becke's three-parameter Lee, Yang, and Parr (B3LYP)[35−37] and the recently released Coulomb attenuating method B3LYP (CAM-B3LYP)[38,39] functionals. The latter has been especially designed to cure the deficiencies of the former in treating charge-transfer (CT) states, and indeed, it was recently found to be the recommended functional for excitation energy calculations, inasmuch as it yields a balanced description of local, Rydberg, and CT excitations.[40] Besides, CAM-B3LYP yielded very good results in our previous studies of linear and nonlinear optical properties on *R*-(+)-3-methylcyclopentanone (R3MCP)[15,41−43] and L-tryptophan,[44] in particular for the high-energy portion of the dichroic spectra. The calculations are carried out in the gas phase and in THF solution. The effect of the solvent onto the TPCD response is investigated within the polarized continuum model (PCM).[45−49] Admittedly, continuum models may be inadequate to describe the effects of solvation, in particular when nonlinear optical processes are studied. Some quite recent experimental evidence[50] has shown the need for more sophisticated models, as those based on quantum mechanics/molecular mechanics methods,[51] also in combination with analytical response approaches,[52,53] to describe the effect of solvent in two-photon absorption.

The theoretical background has been given in detail elsewhere, see refs 11−15 and also refs 43 and 44. The necessary formulas are summarized in the Supporting Information, to which the reader should refer for definitions, symbols, and the convention adopted in this manuscript. Computational Details follow this Introduction. The results of present study are presented and discussed in section 3, whereas section 4 collects our main conclusions.

2. COMPUTATIONAL DETAILS

The geometry of the molecule was taken from ref 54; see Figure 1. It was optimized by the authors of ref 54 at the DFT/B3LYP level,[35−37] using the 6-31+G(d,p)[55] basis set and in the gas phase. A reoptimization with PCM,[45,49] simulating a THF solvation environment, yielded negligible changes, and therefore we employ the original isolated-molecule gas-phase geometry for the main calculations in this work. Later on we will refer to this structure as C_0. The effect of changes of the geometry are further discussed later in the paper. A comparison between the results obtained with the gas-phase optimized 6-31+G(d,p) mentioned just above and those yielded by an alternative geometrical setup is made next using a structure optimized at DFT/B3LYP level with the 6-311++G(2d,2p) basis set[56,57] and kindly provided by Prasad Polavarapu.[58] This second structure will be labeled as C_1. The two geometries are compared in Figure A1 in the Supporting Information, and the major structural parameters are listed in Table A1 thereof.

On the basis of the gas-phase geometry, we computed the OPA, ECD, TPA, and TPCD spectroscopic properties, respectively, at DFT/B3LYP and DFT/CAM-B3LYP[38,39] levels, both

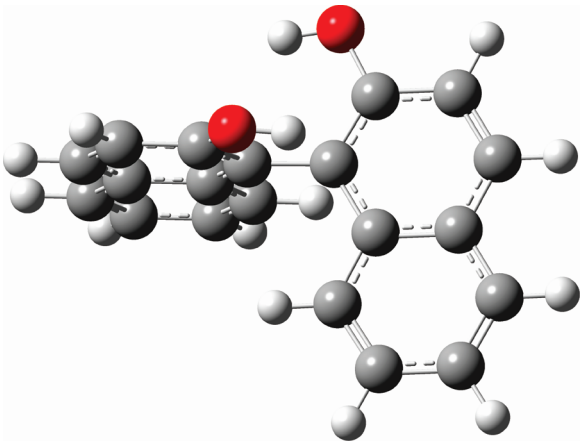

Figure 1. Mlecular structure (labeled C_0 in the text) of R-BINOL.

in the gas phase and in THF. The standard parametrization was used for CAM-B3LYP (α = 0.190, β = 0.460, μ = 0.330). All calculations were carried out with the aug-cc-pVDZ[59] basis set (924 primitives, 632 contracted). This basis set performed nicely in our previous studies of ECD, TPA, and TPCD in amino acids,[11,13,44] helicenes,[14] and R3MCP.[15,41−43] In the gas-phase calculations, labeled GAS/B3LYP and GAS/CAM-B3LYP in the following, the TD-DFT response equations were solved for the lowest 30 excited electronic states. The default convergence thresholds for the residual norm of the response vectors in linear (10^{-4}) and quadratic (10^{-3}) was too tight for uniform convergence through all the 30 excited-state response vectors, and for some of them convergence of the residual norm within the given threshold was not achieved. Nevertheless, the accuracy of the properties (excitation energies and optical responses), as presented here, should be well guaranteed throughout the whole spectrum.

The calculations in PCM, labeled from now on PCM/B3LYP and PCM/CAM-B3LYP, respectively, were carried out with standard atomic radii, according to the united atom topological model,[60] for the cavities: R_C =2.04 Å (with no H bonded), R_C =2.28 Å (CH carbons), R_O =2.22 Å, and R_H =1.44 Å, where the usual multiplicative factor 1.2 is already included. The nonequilibrium regime[61−63] is applied, with the static and optical dielectric constant of 7.58 and 1.971, respectively, for THF. For these calculations we limited our manifold of excited states to the lowest 25, as the combination of hardware limitations and cost made the calculation extended to the lowest 30 states unpractical.

The excitation energies ω_{0f}, the oscillator strengths f_{0f} and the ECD rotatory strength R^{0f}_{ECD} for each electronic state was obtained from the poles and the residues of the appropriate linear response function. The two-photon tensors $S^{0f}_{\alpha\beta}(\omega_{0f})$, $M^{p,0f}_{\alpha\beta}(\omega_{0f})$, $P^{p,0f}_{\alpha\beta}(\omega_{0f})$, and $T^{+,0f}_{\alpha\beta}(\omega_{0f})$ were evaluated from the single residues of appropriate quadratic response functions. The use of London atomic orbitals[64] in ECD[65,66] and of Tinoco's original formulation in TPCD[8,12] implies that these properties are obtained in a form that is origin invariant even for our finite one-electron basis sets.

Conformational analysis upon the rotation of the dihedral angle between the two single naphthols was performed by Boltzmann averaging over a few geometries, where the two naphthyl moieties were rotated from the initial geometry, corresponding to a torsion angle ϑ of 90° (see Figure 1), in both the cisoid ($\vartheta < 90°$) and transoid ($\vartheta > 90°$) conformations without further optimization. The average was obtained using the calculated total energy changes and properties for the different rotamers. The Boltzmann averaged spectrum was then calculated at 298.15 K.

All response calculations were carried out using DALTON 2.0.[67] Gaussian 03[68] was employed for the molecular orbital analysis.

3. RESULTS AND DISCUSSION

As stated in the Introduction, the main motivation of this work is to analyze and discuss the computational challenges faced when TPCD and, in more general terms, nonlinear optical properties of extended chiral systems are studied. Some computational challenges are indeed inherent in the computational complexity of a nonlinear optical process (as TPCD) compared to linear properties, i.e., the need for (a) extended basis set with high cardinal number and a good set of diffuse functions, (b) a reliable electronic structure model that can account for the effect of electron correlation, and (c) the description of quadrupolar and magnetic interaction, with the related problem of gauge origin dependence arising in approximate calculations. These aspects have been discussed in some detail in refs 11−15; see also refs 43 and 44.

Other challenges are more specific of systems exhibiting structural chirality, since these are usually extended and they are characterized by a delocalized electronic structure. Per se they represent in general a challenge for any computational method. Moreover, experimentalists are able to measure chiroptical properties in a large energy range, which enhances the fingerprinting capabilities of the spectroscopic technique. From a physical point of view this means that in extended and delocalized systems a large number of excited states are involved in the measurements. At the state-of-the-art, TD-DFT[33,34] is perhaps the only feasible route to face these challenges, since it offers the best compromise between computational cost and reliability of the results. Nevertheless, to cover the region of frequencies afforded by the experiments, we will show below the results of calculations of the nonlinear optical magnetic and quadrupolar transition matrix elements for quite a few (up to 30) excited electronic states. Simulations of the spectroscopic response of R-BINOL will be performed down to a wavelength of ≈200 nm. The study reaches virtually the limit of what is affordable with current computational resources. With this approach it becomes mandatory to check carefully the "completeness" and convergence of the results, for example with respect to the number of excited states included in the calculations. Another aspect to keep in mind is the fact that BINOL, like many systems built by identical and weakly interacting moieties, may exhibit both localized and delocalized properties. A calculation carried out by taking symmetry into account predicts always a delocalized electronic density. Fluctuations, arising mainly in condensed phase, may be strong enough to overcome the weak coupling and give rise to localized states, with presumably quite different chiral responses. Moreover, localization may appear both in the ground and in the excited electronic states. Delocalized excitonic states can easily evolve into charge-transfer localized states. This has been clearly shown in DNA oligomers,[69,70] and decay through a CT state is now considered as one of the main pathways ensuring DNA photostability.[71,72] Similar phenomena could indeed take place in R-BINOL and traditional hybrid DFT

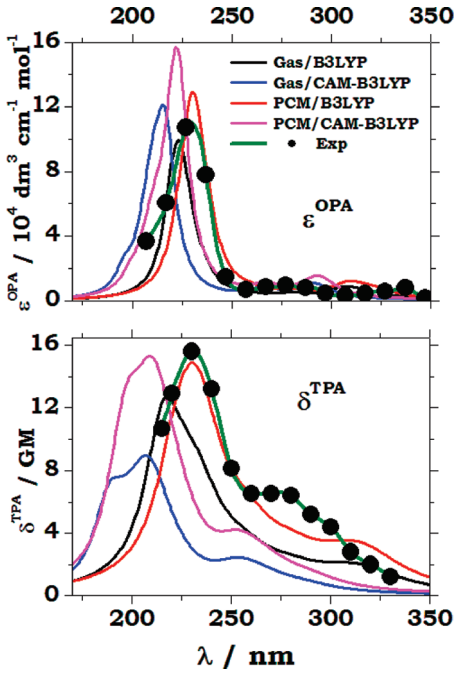

Figure 2. One- (OPA) and two- (TPA) photon absorption spectra of R-BINOL in the region where the first excited electronic states are placed, computed at GAS/B3LYP (black lines), PCM/B3LYP (red lines), GAS/CAM-B3LYP (blue lines), and PCM/CAM-B3LYP (magenta lines) level. The spectra include the response of the lowest 30 excited electronic states in the gas-phase calculations, and of the lowest 25 in the PCM calculations. aug-cc-pVDZ basis set. A line width of Γ = 0.3 eV was used in the convolutions. The corresponding experimental spectra (olive lines) are also given for comparison. They are taken from refs 18 and 19 for TPA (scaling in intensity of a factor of 7.5); from ref 74 for OPA.

functionals exhibit very well-known failure in treating CT states. Quite recently the debate on this point has been revived by the appearance of ref 73, advocating the use of constrained variational DFT for the study of CT transition with standard density functionals.

While the shape of the TPCD signal is nicely reproduced by our simulation, a remarkable discrepancy still exists on the magnitude of the TPCD effect. This aspect will be discussed below. Among the various parameters of the computational study, the possible impact on the computed intensity of the chosen density functional and, to some extent, the effect of conformational freedom will be analyzed. To rationalize the remarkable effect of the introduction of PCM on the spectra, the excited electronic states of R-BINOL are characterized in terms of single excitation between frontier molecular orbitals.

3.1. B3LYP vs CAM-B3LYP; Gas Phase vs PCM. Figure 2 shows the OPA and TPA spectra of R-BINOL calculated at B3LYP/aug-cc-pVDZ and CAM-B3LYP/aug-cc-pVDZ levels both in the gas phase and in THF. In each panel we also show the experimental spectra. OPA experimental data are taken from ref 74, whereas those for TPA were recorded by our group,[16,18,19] and they are scaled by factors of 7.5, so that the intensity at the maximum falls in the range of the corresponding PCM/B3LYP estimates. In Figures 3 and 4 we focus on ECD and TPCD and superimpose the convoluted B3LYP/aug-cc-pVDZ and CAM-B3LYP/aug-cc-pVDZ spectra on the corresponding stick spectra. Figure 3 shows the gas-phase results, whereas Figure 4 is devoted to the simulations carried out in THF, using PCM. In these two figures we also report again experimental ECD data taken from ref 75, whereas TPCD was measured in house,[16,18] and the data are scaled in intensity by a factor of 350. In Figures 3 and 4 the experimental curves are shifted in the wavelength scale to maximize the overlap with our simulated spectra. Experiment is not reported in the panel of Figure 3 showing GAS/B3LYP ECD results, since in this case the computed spectral profile is clearly far off the experimental one, and a comparison has little meaning. Preliminary results for TPCD, obtained at B3LYP/aug-cc-pVDZ level, were already shown in ref 18.

A Lorentzian line width Γ of 0.3 eV was employed for all excited states and for all properties to broaden the vertical transition properties. In the range of wavelengths considered in the figures (170−350 nm) the line widths vary between 7 and ≈40 nm. The data used to draw the spectra are summarized in Table A2 of the Supporting Information, which reports the excitation energies (ω_{0f}, in eV and λ_{0f}, in nm); the TPCD parameters $B_1^{TI}(\omega_{0f})$, $B_2^{TI}(\omega_{0f})$, and $B_3^{TI}(\omega_{0f})$; the TPCD rotatory strength $R_{0f}^{TPCD}(\omega_{0f})$ for two circularly polarized light beams aligned parallel to each other and copropagating; the TPA parameters $\mathscr{A}(\omega_{0f})$ and $\mathscr{B}(\omega_{0f})$ with the TPA transition probability $\bar{\delta}_{0f}^{TPA}(\omega_{0f})$ computed for LP light; the ECD rotatory strength R_{0f}^{ECD}; and the OPA oscillator strength f_{0f}, with data covering the full set of excited electronic states for each of the four combinations of phase/density functional. For each one of the excited electronic states included in the analysis, the label (A or B) of the C_2 point symmetry group to which the molecule belongs is given. It can rather trivially be proven that the $\mathscr{A}(\omega_{0f})$ and $B_3^{TI}(\omega_{0f})$ molecular parameters (see eqs 4 and 9 in the Supporting Information), involving products of traces of (electric dipole moment, magnetic dipole moment, and velocity) two-photon tensors, vanish identically for final electronic states of B symmetry (the ground state being totally symmetric). In Table 1 the areas of the spectra are given as the sum over the rotatory strengths R_{0f}^{ECD} (ECD) and $R_{0f}^{TPCD}(\omega_{0f})$ (TPCD), over the ratios f_{0f}/ω_{0f} (OPA), and the two photon probabilities $\bar{\delta}_{0f}^{TPA}(\omega_{0f})$ (TPA). For ECD and TPCD we report the actual areas (sum of rotatory strengths) and the absolute areas (sum of the absolute values of the rotatory strengths). For the gas-phase calculations the results obtained summing over the whole 30 excited states and those given by a sum over the first 25 are given. We also show in Table 1 how the different sums split between states of A and B symmetry (see footnotes).

For all spectra under study, CAM-B3LYP yields profiles that are blue-shifted with respect to those predicted by B3LYP. This is consistent with our previously reported results on R3MCP.[15,41−43] and in line with the recent literature,[76,77] since most of the states described are essentially valence states with dominant contributions from $\pi \rightarrow \pi^*$ excitations. Moreover, CAM-B3LYP gives, for both OPA and ECD, larger intensities than B3LYP, in particular in the gas phase. The integrated absolute intensity (for N = 30) in the GAS/CAM-B3LYP ECD spectrum (see Table 1) is indeed 46% greater than that of the corresponding GAS/B3LYP one, whereas the enhancement is approximately 34% if we compare in a similar way the OPA spectra. Percentages of about 34 and 26, respectively, are obtained when the analysis is carried out on the PCM spectra. Note that the GAS percentages double if we take only the first 25 excited states in the summations (N = 25, see Table 1). The situation is quite different for TPCD, where the integrated absolute intensities are slightly lower for CAM-B3LYP than B3LYP, by approximately 2%, for the gas-phase simulation

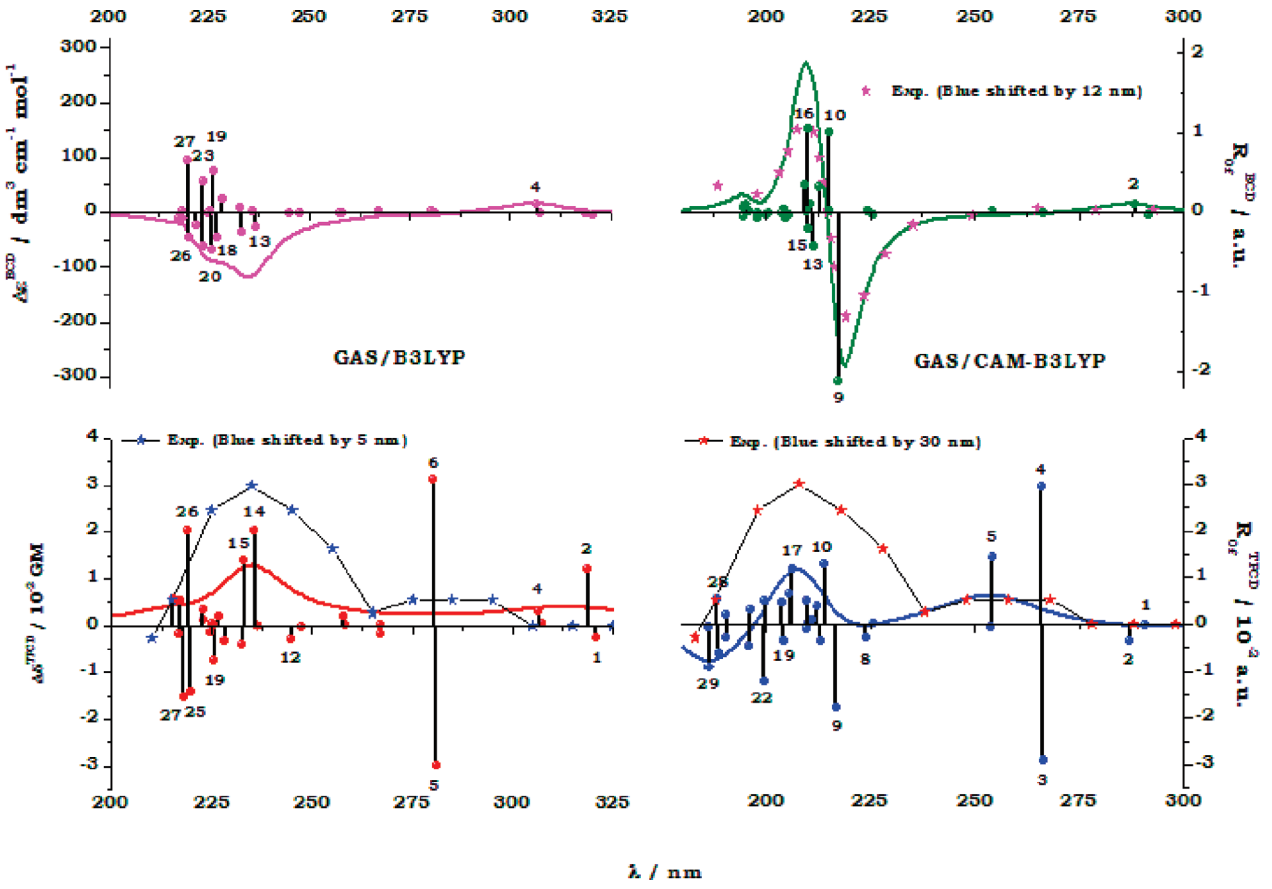

Figure 3. One- (ECD) and two-photon (TPCD) circular dichroism spectra of R-BINOL in the region of the first 30 excited electronic states, computed both at GAS/B3LYP/aug-cc-pVDZ and at GAS/CAM-B3LYP/aug-cc-pVDZ levels. Both the stick spectra and the spectra convoluted with a line width of 0.3 eV are shown. Except for the upper left panel, the experimental spectra are superimposed. They are shifted in the wavelength axis as indicated, to optimize the overlap with the simulations. The ECD spectrum is taken from ref 75; the TPCD spectrum is taken from ref 18, and it is scaled in intensity by a factor of 370.

(N = 30), whereas they are larger by ∼25% for the PCM one. Once again a major role is taken by the frontier excited states: indeed, by restricting the sum to the lowest 25 excited electronic states of the gas-phase calculations, an enhancement in the integrated absolute TPCD intensities is observed (approximately 13%). As far as the TPA spectra are concerned, the difference in integrated intensity between B3LYP and CAM-B3LYP is slightly in favor of the former: CAM-B3LYP integrated intensities are 31% (GAS) and 12% (PCM) lower than the corresponding using B3LYP. These percentages change for TPA spectra as a result of the use of circularly polarized photons (15% and 20%, respectively, results not shown).

If we limit our analysis only to the effect of the first 25 excited states, integrated intensities in the range of wavelengths reported in the Figures are always negative for ECD, but with negative and positive rotatory strengths almost fully compensating each others. Indeed, the cancellation between large positive (mostly related to A excited states) and negative (mostly B excited states, see footnote in Table 1) is very strong, except perhaps for the GAS/B3LYP calculations. In TPCD the integrated intensities are instead always positive, and yet again states of A symmetry are mostly associated with positive rotatory strengths, whereas those of B symmetry associate mainly with negative rotatory strengths. We will come back to this point later. Note also that, when integrated intensities obtained with the first 25 excited states are compared with those yielded by all 30 states in the gas-phase calculations, it can be seen that the extra five states (the 26th to the 30th) have a remarkable effect in the GAS/B3LYP case, increasing for instance the integrated intensity in TPA by as much as 58%. The effect is more contained for CAM-B3LYP (only 19% increase in the TPA integrated intensity upon extension of the number of excited state from 25 to 30).

It is also interesting to highlight that integrated intensities are invariably enhanced upon solvation.

3.2. Comparison with Experiment. If we leave out for a moment the issue of the relevant discrepancy occurring for the intensity of the TPA signal, which is underestimated by a factor of 7.5, and even more strikingly for TPCD, which is estimated a factor of 350 times weaker than measured, and focus on the line shapes of the spectra, we can safely state that, with the exception of the ECD spectrum computed at B3LYP level, our simulated spectra, for one- and two-photon processes, are in rather good agreement with the experiment, independent of the computational approach (see Figures 2−4).

Absorption Spectra. All models reproduce well the profiles of the experimental OPA and TPA spectra. In particular, the position and shape of the maxima of absorption (located around 230 nm) are reproduced well by the PCM/B3LYP calculations (red curves in Figure 2). The weaker maxima observed in both OPA and TPA around 280 nm, on the other

dx.doi.org/10.1021/jp108669f |J. Phys. Chem. B 2011, 115, 811–824

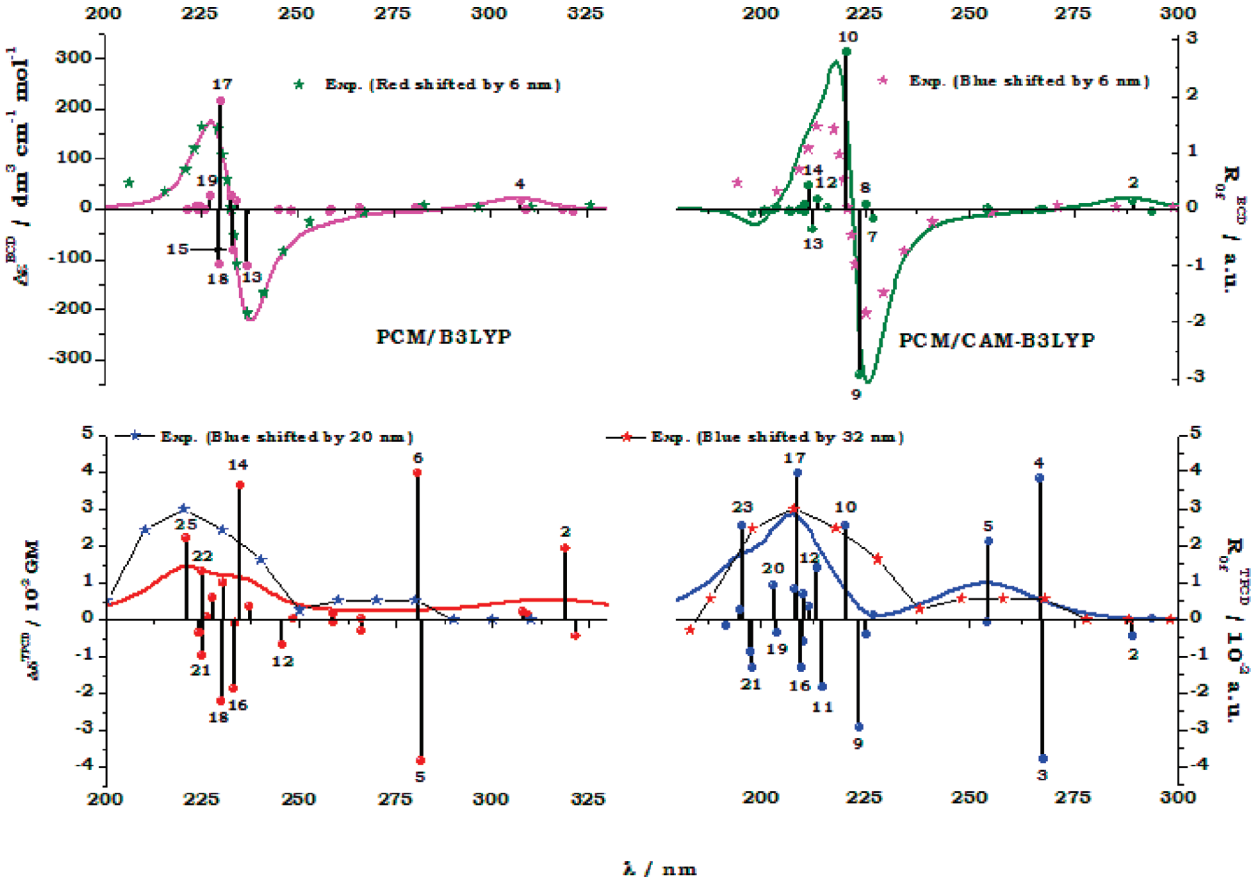

Figure 4. One- (ECD) and two-photon (TPCD) circular dichroism spectra of R-BINOL in the region of the first 25 excited electronic states, computed both at PCM/B3LYP/aug-cc-pVDZ and at PCM/CAM-B3LYP/aug-cc-pVDZ levels. Both the stick spectra and the spectra convoluted with a line width of 0.3 eV are shown. The corresponding experimental spectrum are superimposed. They are shifted in the wavelength axis as indicated, to optimize the overlap with the simulations. The ECD spectrum is taken from ref 75; the TPCD spectrum is taken from ref 18, and it is scaled in intensity by a factor of 370. PCM is employed to simulate solvation in THF.

Table 1. Measures of the Areas of the OPA, ECD, TPA, and TPCD Spectra (au)[a]

	$\Sigma_{j=1}^{N}(f_{0f})/(\omega_{0f})$[b]	$\Sigma_{j=1}^{N}R_{0f}^{ECD}$[c]	$\Sigma_{j=1}^{N}\lvert R_{0f}^{ECD}\rvert$[d]	$\Sigma_{j=1}^{N}\bar{\delta}_{0f}^{TPA}(\omega_{0f})$[e]	$\Sigma_{j=1}^{N}R_{0f}^{TPCD}(\omega_{0f})$[f]	$\Sigma_{j=1}^{N}\lvert R_{0f}^{TPCD}(\omega_{0f})\rvert$[g]
GAS/B3LYP	8.80 (11.1)	-6.58×10^{-1} (-4.73×10^{-1})	3.20 (4.34)	2.82×10^{4} (4.45×10^{4})	4.24×10^{2} (7.06×10^{2})	3.25×10^{3} (4.24×10^{3})
GAS/CAM-B3LYP	14.2 (14.9)	-8.17×10^{-2} ($+1.79\times10^{-2}$)	6.11 (6.36)	2.55×10^{4} (3.04×10^{4})	3.49×10^{2} (1.84×10^{2})	3.69×10^{3} (4.17×10^{3})
PCM/B3LYP	14.9	-7.71×10^{-2}	5.64	5.67×10^{4}	9.49×10^{2}	5.51×10^{3}
PCM/CAM-B3LYP	18.8	-7.64×10^{-2}	7.55	4.99×10^{4}	1.06×10^{3}	6.90×10^{3}

[a] Data obtained summing upon the lowest twenty five excited electronic states ($N = 25$). In parentheses, for the gas-phase calculations only, the values resulting by a summation upon all thirty excited electronic states employed in these calculations ($N = 30$). Atomic units. [b] The sum, extended over all states, splits as follows between A and B symmetry states: 4.02 (A), 7.05 (B) for GAS/B3LYP; 6.20 (A), 8.74 (B) for GAS/CAM-B3LYP; 5.53 (A), 9.39 (B) for PCM/B3LYP; 7.52 (A), 11.22 (B) for PCM/CAM-B3LYP. [c] The sum, extended over all states, splits as follows between A and B symmetry states (in units of 10^{-3} au): +50.42 (A), −523.2 (B) for GAS/B3LYP; +2453 (A), −2435 (B) for GAS/CAM-B3LYP; +2748 (A), −2825 (B) for PCM/B3LYP; +3546 (A), −3622 (B) for PCM/CAM-B3LYP. [d] The sum, extended over all states, splits as follows between A and B symmetry states (in units of 10^{-3} au): 1733 (A), 2603 (B) for GAS/B3LYP; 2880 (A), 3475 (B) for GAS/CAM-B3LYP; 2767 (A), 2870 (B) for PCM/B3LYP; 3758 (A), 3796 (B) for PCM/CAM-B3LYP. [e] The sum, extended over all states, splits as follows between A and B symmetry states: 35920 (A), 8625 (B) for GAS/B3LYP; 22200 (A), 8170 (B) for GAS/CAM-B3LYP; 44700. (A), 12020. (B) for PCM/B3LYP; 38250 (A), 11630 (B) for PCM/CAM-B3LYP. [f] The sum, extended over all states, splits as follows between A and B symmetry states: +1554 (A), −847.8 (B) for GAS/B3LYP; +1038 (A), −854.9 (B) for GAS/CAM-B3LYP; +2456 (A), −1507 (B) for PCM/B3LYP; +2678 (A), −1617 (B) for PCM/CAM-B3LYP. [g] The sum, extended over all states, splits as follows between A and B symmetry states: 2373 (A), 1867 (B) for GAS/B3LYP; 2359 (A), 1815 (B) for GAS/CAM-B3LYP; 3667 (A), 1842 (B) for PCM/B3LYP; 4287 (A), 2609 (B) for PCM/CAM-B3LYP.

hand, are apparently red-shifted by about 35 nm in the PCM/B3LYP calculations. The experimental separation (of ca. 50 nm) between the two maxima is better reproduced by the PCM/CAM-B3LYP calculations, in magenta in Figure 2, and (perhaps to a lesser extent) by the GAS/CAM-B3LYP calculations, in blue in Figure 2, which, on the other hand, yield peaks blue-shifted by about 30 nm. For a more in depth discussion of the comparison between theory and experiments for TPA the

reader should refer to ref 19, where the TPCLD of BINOL was analyzed in detail.

Note that while for the OPA spectrum, the excited states of B symmetry contribute to about 57−63% of the overall transition strength, depending on the computational model (see Table A1 in the Supporting Information and Table 1), their contribution drops to 19−27% for TPA. This shows the extent to which symmetry selection rules are partially working for BINOL. These selection rules cannot be rigorous in BINOL, due to its relatively low symmetry, but they are nevertheless apparently reasonably effective. Note also, as with the some relevant exceptions (see, as an example, state 13 in the PCM/B3LYP calculation, or state 9 in the PCM/CAM-B3LYP), states that yield significant TPA contributions display low activity in OPA, and vice versa.

CD Spectra. From now on in this section we turn to the CD spectra, shown in Figures 3 and 4. In general, CD (ECD and TPCD) is more sensitive to the solvent environment than the related absorption. The broad negative band in the short wavelength region of the ECD profile in the GAS/B3LYP calculation (upper left panel, Figure 3) splits into two peaks of opposite sign and of comparable intensities when the effect of the THF solvent is accounted for by PCM (PCM/B3LYP results, upper left panel, Figure 4). This difference is of major relevance since, as shown in Figure 4, the PCM/B3LYP results are in excellent agreement with the experiment, while the GAS/B3LYP results are clearly far from it. Systems such as BINOL are characterized by a high density of high lying excited states with strong dichroic response. Note, for instance, that if one would restrict the analysis to only the lowest 25 states, the GAS/B3LYP TPCD spectrum (with the chosen phenomenological line width) would show a broad negative band extending from 170 to 240 nm, with a sign opposite to the one observed in all cases in both Figures 3 and 4. Indeed, the 26th state displays a strong positive rotatory strength (see lower left panel in Figure 3) that upon convolution, is sufficient to change sign to the whole band below 250 nm. Note also that GAS/CAM-B3LYP calculation, carried out with 30 excited states, yields a TPCD spectrum that not only reproduces the main positive experimental band at about 210 nm (computed value) but also shows a change of sign at the lowest end of the wavelength axis, something that seems to get along well with the experiment (see lower right panel of Figure 3), and which is absent in the lower panels of Figure 4.

These results clearly highlight the challenges arising from the need of a proper accounting not only for the environmental effects but also for the completeness of the excited-state manifold. In systems such as BINOL the density of excited electronic states is quite large in the area where the CD is particularly strong. The description of high lying excited states is particularly challenging also due to the fact that, approaching the ionization threshold of the HOMO Kohn−Sham orbital, spurious mixing with ionic states may arise.[78,79] This problem is less serious with a long-range corrected hybrid functional as CAM-B3LYP, where the HOMO energy is usually lower than that using a standard hybrid functional like B3LYP. In our calculations indeed the Kohn−Sham HOMO orbitals rest at ca. 5.93 eV below the ionization threshold in the B3LYP calculations (both GAS and PCM), about 0.2−0.3 eV above the excitation energy of our highest lying excited electronic states. The Kohn−Sham HOMO in the CAM-B3LYP calculations is sensibly lower, ca. 7.21 eV. This extends the energy range that can be reliably explored by the TD-DFT method. In the specific case, the simulated spectra are expected to be free from spurious effects related to ionized states, since the energy of the HOMO is about 0.6−0.8 eV above the excitation energies of our frontier excited states.

If the PCM/B3LYP ECD spectrum is (except for a mere 6 nm red shift) essentially overlapping the experimental curve of ref 75, CAM-B3LYP curves are very close to experiment, being both blue-shifted by only a few nanometers and only slightly more intense than experiment. The GAS/CAM-B3LYP calculation reproduces also the weak maximum around 200 nm seen in the experiment (see Figures 2 and 3). This happens due to the inclusion of excited electronic states not affordable at this stage in our PCM calculations.

The pairing nature of the dichroic response is well evident from the data in Table A1 in the Supporting Information and from the stick spectra in Figures 3 and 4. Both ECD and TPCD rotatory strengths come in pair, often of opposite sign. The observed pattern in ECD, with the dispersion Fano-type profile, is the result of the combination of strengths attributable to the cluster of excited electronic states beyond the twelfth excited state according to B3LYP. In the gas-phase calculation all excited states beyond the 12th do mix, with a net prevalence of negative response, therefore missing the experimental profile. In the condensed-phase simulation, the positive contribution of the 17th state is dominating, yielding a positive lobe on the spectrum in the blue region of the spectral range between 240 and 220 nm. States 13 and 15 combine to yield the negative lobe in the red portion of the same region, while the negative contribution of state 18 attenuates the effect of the positive rotatory strength of state 17. In the CAM-B3LYP spectra, the ninth state is responsible for the negative peak, whereas the positive peak is due to the combination of rotatory strengths of state 10 (PCM) and states 10 and 16 (GAS).

It is worth noting, again, that the most intense positive rotatory strengths belong to states of A symmetry, whereas negative rotatory strengths are most often related to states of B symmetry. This occurrence can also be verified for the TPCD spectra. Indeed, the splitting of positive and negative rotatory strengths between A and B states is very high in particular for ECD (see comparison between direct sums and sums of absolute rotatory strengths in Table 2, where $|\Sigma_{f\subset A \text{ or } B} R_{0f}^{ECD}| \approx \Sigma_{f\subset A \text{ or } B} |R_{0f}^{ECD}|$ except for the GAS/B3LYP calculation).

Two-Photon CD. All TPCD calculations are in qualitative agreement with the experiments, if we leave the intensity issue out and apply appropriate shifts on the wavelength axis. The maxima (lying in experiment at $\lambda \approx 240$ nm) are all blue-shifted by values ranging from 5 nm (GAS/B3LYP) to ≈30 nm (both CAM-B3LYP calculations). CAM-B3LYP better reproduces the energy separation between the most intense blue peak and the red-shifted peak/shoulder (about 50 nm, see also discussion of TPA, above). This evidences a more balanced description of the electronic states involved in the experimental spectra. While both PCM calculations yield a double-peak structure partially hidden below the stronger blue peak, PCM/B3LYP is the only method that reproduces the experiment with respect to the peak at low wavelength; i.e., the mentioned peak is more intense than the following one at longer wavelengths. As mentioned above, the negative rotatory strengths of states above the 25th yield a negative TPCD signal below 200 nm in the GAS/CAM-B3LYP spectrum. This feature is present in experiment but absent in the PCM calculations, which are limited to twenty five excited electronic states.

As far as the distribution of the TPCD rotatory strength is concerned, it is interesting to note that the shallow plateau

observed at approximately 300 nm in the experimental spectrum, hides, according to our B3LYP calculations, the contribution of the first and second excited electronic state (the latter largely dominating) while the large rotatory strengths of the fifth and sixth excited states cancel each other very efficiently. The scenario is similar with CAM-B3LYP. However, using this functional we find that the two states whose rotatory strengths cancel each other are instead the third and fourth, whereas the largest contribution to the shallow maximum comes from the fifth state. Therefore, the plateau is the result of the efficient partial cancellation of strong rotatory strengths of states of opposite symmetry but virtually equal intensity. The same can be said for the spectral broad band extending below 250 nm, which again results from a very efficient cancellation of rotatory strengths between pair of states of opposite symmetry. The order of the states changes from the gas to the condensed phase. Consequently, from B3LYP to CAM-B3LYP, the rotatory strengths are reshuffled essentially among all states above the 11th state for B3LYP or the seventh state for CAM-B3LYP, up to the last excited state involved in the calculation.

The comparison with the experimental spectra shows that CAM-B3LYP, which is a version of B3LYP tailored to describe charge-transfer excitations and long-range dispersion effects, and which was proven to be very effective in describing the low-wavelength portion of the spectra of R3MCP in our previous studies,[15,41−43] performs somewhat better than B3LYP, provided that PCM is employed, in reproducing both the overall ratio of intensities and the separation between the main peak centered at about 240 nm in experiment and the weaker maximum located around 280−300 nm. Also, CAM-B3LYP in the gas phase appears to be able to reproduce the inversion of sign observed in the experiment at the lowest wavelength edge of the spectrum. However, it misses the order in intensities between main peak and shoulder for the broad low-wavelength band thus yielding, not unexpectedly, a larger blue shift of the whole TPCD spectrum. The latter is due to the overestimation of the excitation energies partially mitigated by an evident redistribution of the rotatory strengths throughout the range of the spectrum. This redistribution is far more efficient in the ECD spectrum, where experimental and theoretical spectra can be compared directly, without needing scaling, and where, in spite of the overestimation of the excitation energies, the PCM/B3LYP and PCM/CAM-B3LYP are equally (and oppositely) shifted by only 6 nm with respect to experiment. In addition, the former appears to be performing better than the latter since it reproduces remarkably well the intensity of the signal. Note that the different blueshift of the computed values with respect to experiments in ECD and TPCD spectra is not unphysical, since these are dominated by different molecular states. In the specific case of BINOL, the accurate calculation of the states relevant for the two-photon spectra appears to be more challenging than that of the states dominating the one-photon properties.

At the end of this section, we are left with the task of trying to find a theoretical justification for the large disagreement between calculations and experiment on the intensity of TPA and, even more important, TPCD. Possible causes for what might be read as a huge underestimation of the TPCD signal by our computational approach are, in our view, attributable essentially to two possible causes: (i) the typical excitonic, i.e., pairing structure of excitation spectrum of BINOL, where a strong cancellation between rotatory strengths of nearly degenerate states of different symmetry exists; (ii) the possible insurgence of conformational effects, which can perturb this balance. We discuss the second point in the next section. As for the first possible cause, we note that the sum of the absolute values of the rotatory strengths for TPCD (5510 au) is about 6-fold that of the direct sum (949 au) of the TPCD spectrum. This shows that a great amount of the TPCD rotatory strength is lost in the positive/negative alternation of signs. As a consequence, "minor" changes in the placement of the excited electronic states and/or in the strength of the response might yield in principle major changes in the TPCD spectrum, thus possibly influencing the overall intensity. On the other hand, disagreements of 2−3 orders of magnitude cannot be rationalized easily, since indeed the sum of absolute intensities yielded by our simulation is at the most only 6 times larger than the direct sum of intensities. Even if it must be stressed that when states mix, they mix via their transition amplitudes and not via their transition probabilities, and possible interferential effects (responsible for example of the superradiance phenomenon[80]) may arise, on the grounds of the analysis given above it is difficult to imagine that possible mixings of the states may explain the 2 order of magnitude stronger intensity observed experimentally in TPCD. Moreover, the shape of the spectrum is, in our calculations, overall in rather nice agreement with experiment, and, last but not least, our computational approach yields an excellent agreement, considering both intensity and shape, for the ECD spectrum of BINOL.

In the following we will try to analyze in some way the possibility of huge unaccounted for conformational and/or excitonic effects. Since no decisive argument for preferring one functional over the other could be introduced in the discussion above, we choose to focus on the PCM/B3LYP results for the remaining analysis.

3.3. Rotation of the Dihedral Angle. The geometry optimizations in both the gas phase and THF show that the conformation in which the two naphthol moieties of BINOL are perpendicular to each other, with the dihedral angle of about 90°, and the two hydroxyls are pointing to the other naphthol is energetically favored (see Figure 1).

Nevertheless, it is reasonable to expect that the torsion of the dihedral might be only partially hindered, and this might have a relevant impact on the optical responses, thus altering the excitonic interactions between the π systems of the two moieties. Also, a recent study[81] has shown that the charge-transfer character of the excited states of Pigment Yellow 101, a system whose structure is somewhat similar to that of BINOL, changes substantially upon twisting of the geometry around the single C═N−N═C bond linking the two naphthol moieties. To investigate if a slow scissoring motion of the two naphthols could explain, in part and in a simple way, the drastic difference in the intensity between the measured and simulated TPCD spectra, we performed simulations of the spectra for conformers of R-BINOL where the torsion angle ϑ was modified, assuming values of ±75° and ±60°. Larger torsions led to steep increases of the total energy of the conformers and were not taken into account. The calculations were carried out at the PCM/B3LYP/aug-cc-pVDZ level, and were *not* preceded by further geometry reoptimization: the structure C_0, employed for the single point calculations discussed above, was simply subject to torsions of the dihedral angle. Boltzmann averages were performed by employing weights derived from total energies. In Figure 5, the Boltzmann-averaged spectra are shown together with the individual conformer contributions already scaled by the Boltzmann weights. The latter are given in the inset. At each value of the

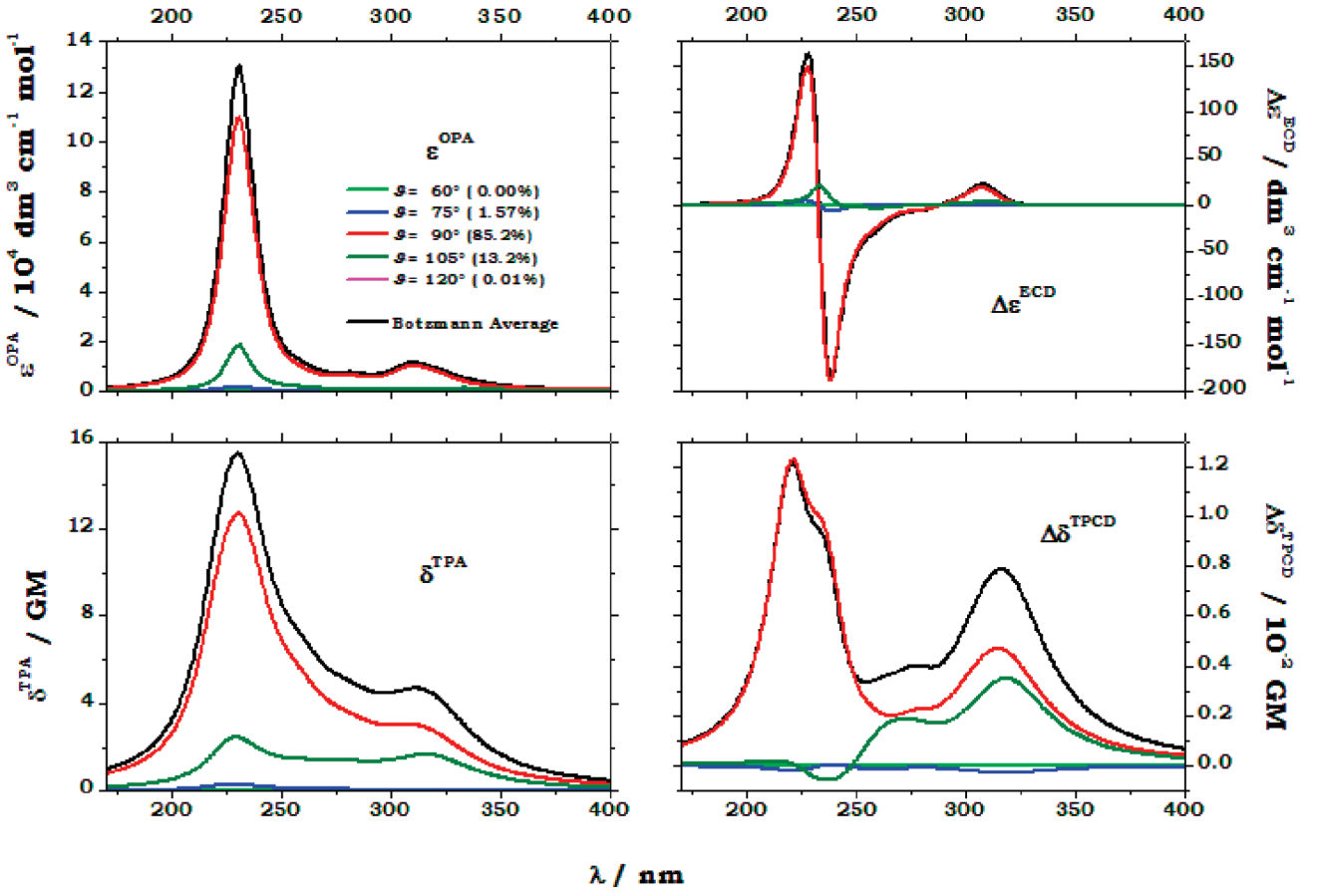

Figure 5. One- (ECD) and two-photon (TPCD) circular dichroism, one- (OPA) and two-photon (TPA) absorption spectra of R-BINOL in the region of the first 25 excited electronic states, computed at the B3LYP/PCM/aug-cc-pVDZ level in THF, for geometries with different dihedral angles ϑ between the two naphthols. The Boltzmann averaged spectra are also given. See text for details.

wavelength, the thick black curve is the algebraic sum of the thinner colored values. The data in the lower right panel of Figure 5, referring to TPCD, were shown already in ref 18.

It is rather clear from Figure 5 that the reference conformer, corresponding to torsion angle of 90°, dictates in all cases the overall behavior. The conformers corresponding to a torsion angle varied by ±15°, in particular the one in a transoid conformation (ϑ = 105°) yields relevant contributions without modifying the structure of the two absorption spectra. Larger torsions yield contributions which, if detectable, are nevertheless much less substantial. Note in the TPCD spectrum of Figure 5 the transoid conformer (ϑ = 105°) is responsible for the change in the structure of the spectrum between 230 and 250 nm, where it shows a non-negligible negative contribution to the average.

In summary, the effect of the twisting motion of the two naphthols, accounted through this admittedly rather crude but reasonable approximation, is quite limited and, as can be seen by a comparison between the spectra of Figure 5 and the experimental data reported in Figures 2 and 4, definitely not sufficient to account for the large discrepancies between measured and computed intensities in the two-photon spectroscopies (see scaling factors mentioned in section 3.1).

Inspection of Figure 1 suggests that the rotation of the hydroxyl groups may reduce the steric hindrance and consequently enhance the molecular flexibility along ϑ, with possible effects of the coupled motions along ϑ and the rotation of the hydroxyls. A full multidimensional exploration of the potential energy surface would be very demanding from the computational point of view. To investigate this possible effect, we adopted a more convenient strategy, performing exploratory calculations on the geometries (of S-BINOL) kindly provided by Prof. Polavarapu,[58] These structures, corresponding to three different conformers with torsion angle ϑ = 90°, were originally optimized at B3LYP/6-311++G(2d,2p) level in the gas phase. The three conformers differ for rotations of the two hydroxyl groups. In conformer C_1 the latter were arranged exactly as in Figure 1. Figure 6 shows the stick ECD and TPCD spectra computed, in a PCM/B3LYP approximation employing the aug-cc-pVDZ basis set for conformer C_1, compared to those obtained with our geometrical setup, conformer C_0, and already reported in the right panels of Figure 4. The differences between the responses (both linear and nonlinear) of the two structures are quite small, and mostly arising from minor redistribution of intensities within the manifold of excited states lying below 250 nm. Conformer C_2 differs from C_1 in the position of one of the hydroxyls, which is rotated by 180°, toward its own naphthol moiety. In conformer C_3 both −OH groups are rotated by 180°. These structures, where presumably the steric hindrance related to the change in the torsion angle ϑ should be less pronounced, were nevertheless found to be significantly less energetically favored than the reference structure used throughout this work. Moreover, their TPCD spectra (not shown here) are very similar to those obtained with conformer C_1, which leads us to conclude that neither changes in the geometry nor conformational effects

dx.doi.org/10.1021/jp108669f |J. Phys. Chem. B 2011, 115, 811–824

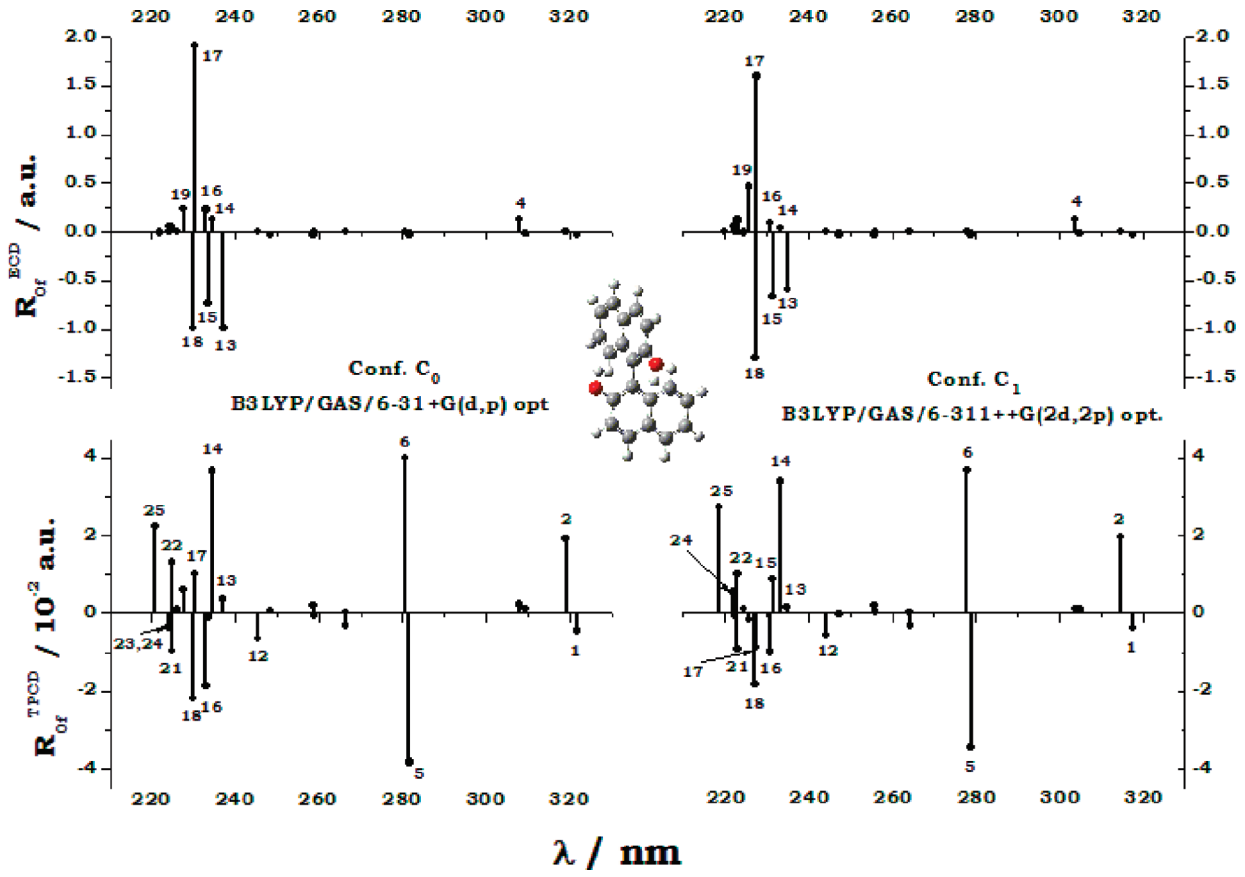

Figure 6. One- (ECD) and two-photon (TPCD) circular dichroism stick spectra of R-BINOL in the region of the first 25 excited states, computed at B3LYP/PCM/aug-cc-pVDZ level for the geometry of ref 54 (optimized at the B3LYP/GAS/6-31+G(d,p) level, left panels) and for that provided by Prof. Polavarapu[58] (optimized at the B3LYP/GAS/6-311++G(2d,2p) level, right panels).

connected with the variation of the torsion angle between the two naphthyl moieties seem to be able to modify the overall appearance of the linear and nonlinear dichroic spectra, and even less the intensity of the signal. In conclusion, the analysis of the most likely causes related to the computational approximations adopted in our studies for the disparity in intensities between experiment and theory in the TPA and TPCD spectra leads, in our view, to the assumption that such a discrepancy has other origins, and it is due, to a significant degree, to the pulse width of the laser used during the measurements.[18]

3.4. Assignment of the Excited States. In this section we present an analysis of the excited states of BINOL in terms of the relevant single excitations between molecular orbitals. We aim at a characterization of the states responsible for the one- and two-photon responses, unveiling the physical origin of the structure "in pairs" of the spectra, seen, as highlighted in the previous sections, especially in the high wavelength region. This analysis will introduce another computational challenge of the present study, related to the possible existence of CT states, partially hidden by symmetry. The data employed for the analysis are the elements of the TD-DFT excitation vectors reported in Table A3 of the Supporting Information, where, in Figure A2, the molecular orbitals involved in these excitations are also shown. The study was carried out using Gaussian 03[68] at GAS/B3LYP/aug-cc-pVDZ and PCM/B3LYP/aug-cc-pVDZ levels, and it was limited to the lowest 25 excited electronic states. In these calculations, contrary to those properties carried out without symmetry with DALTON 2.0,[67] the code detects symmetry C_2. The differences found in excitation energies and oscillator strengths using Gaussian 03 and DALTON 2.0 are ascribed mainly to the differences in the implementations of Gaussian 03 and DALTON 2.0, both in the form of the functional and in the PCM routines. Due to these differences, the direct one-to-one comparison of excited states between data in Table A3 and those in Table A2 of the Supporting Information is not trivial for states in the higher excitation energy range. The excitations are then given as HOMO$-x\rightarrow$LUMO$+y$, associating the corresponding entry in the TD-DFT excitation vector. Only excitations with vector coefficient values larger than 0.1 are reported. The "de-excitation" part associated to the random-phase approximation structure of the excitation vector is neglected.[14,15] As already proven, e.g., in refs 14 and 15, this is a very reasonable approximation for low lying excited states. Therefore, the sum of the squares of the coefficients given in Table A3 (Supporting Information) adds up to $1/(2)^{1/2}$ instead of 1 (as normalization to unity should imply). The sum of all squared coefficients provides a good estimate of the contribution of the vast number of remaining excitations left out in the calculation.

From Figure A2 (Supporting Information) it can be seen that the molecular orbitals up to LUMO+4 apparently involve $\pi\rightarrow\pi$ excitations of the two rings, mixing rather localized orbitals. Only above LUMO+4 the orbitals start to be diffuse, which explains the satisfactory performance of B3LYP compared to CAM-B3LYP.

The analysis in terms of molecular orbitals yields further insight into the solvent effect on the excited states of R-BINOL.

dx.doi.org/10.1021/jp108669f |J. Phys. Chem. B 2011, 115, 811–824

In fact, apart from sign, the molecular orbitals from HOMO−6 to LUMO+11 are very similar in the gas and condensed phase, with the only exception of the exchange in order of increasing energy of LUMO+8 and LUMO+9. A direct comparison of the excited states, is therefore possible by an analysis of the main contributions reported in Table A3 (Supporting Information). Up to state 12, a one-to-one assignment of the excited states in the two phases can be made. In this first part of the spectrum, excited states are very similar, have the same symmetry, and have very similar excitation energies and the paired structures of the spectrum, with tiny energy gaps between the pair, are almost the same. Remarkably, these minor differences can modify substantially the optical response. Often, moving from gas to condensed phase, for these low lying excited states, an increase of the one-photon oscillator and rotatory strength by a not dissimilar amount is seen, suggesting an increase in the electric transition dipole length. TPCD follows a similar behavior, albeit with a somewhat larger sensibility to small changes in the excited-state wave function. At higher energies the one-to-one comparison of the states in gas and THF solution becomes more and more difficult as a result of a progressive mixing of the states that causes large differences in the optical responses. This mixing is not surprising if one notices that about 13−14 states lie in a very narrow energy window of approximately 0.4 eV (from 5.2 to 5.6 eV). In such a situation, even a moderate perturbation due to the surrounding solvent altering either the energies or the couplings of the main excitations in the excitation vectors can result in very different final eigenstates. In such a situation, it is very likely that nuclear displacements may affect the states-mixing, thus strongly suggesting the existence of relevant vibronic effects on the optical response in this energy window. Due to quasi degeneracy of the states, an ab initio vibronic treatment of the problem would require a variational approach, and not a simple perturbative Herzberg−Teller treatment like those we presented for TPCD response in refs 41−43. Unfortunately, a variational treatment for such highly excited states and in such a complex system, is, at the state-of-the-art, out of reach. It is nevertheless comforting that a pure electronic treatment is still able to provide a reasonable qualitative agreement with experiments (we will comment later on whether vibronic couplings may be responsible for the large discrepancy in the intensity of the TPCD signal as measured and predicted theoretically).

Excited states of R-BINOL appear as pairs, due to the weak interaction between the two naphthols arranged perpendicular to each other. An analysis of the excited states of R-BINOL can therefore also be made considering interacting individual naphthol moieties. The molecular orbitals of 1-naphthol, obtained with the same model and basis set used to obtain the orbital of R-BINOL displayed in Figure A2, are shown in Figure A3, again to be found in the Supporting Information. A comparison of Figures A2 and A3 shows that HOMO−5 and HOMO−4 of R-BINOL emerge from the symmetric and antisymmetric combination of the HOMO−2 of the two single naphthols. In the same way, HOMO−3 and HOMO−2 of R-BINOL emerge from HOMO−1 of the two single naphthols, while HOMO−1 and HOMO emerge from HOMO and LUMO and LUMO+1 emerge from LUMO. A similar analysis applies also to the other molecular orbitals.

This structure in pairs is of help for further analysis of the excited states of R-BINOL. Let us focus on the first four excited states, for which the analysis is understandably easier. Inspection of Table A3 (Supporting Information) shows that they mainly arise from HOMO → LUMO and HOMO−1 → LUMO+1 excitations (the first and the third, of B symmetry and bright for OPA) and from HOMO−1 → LUMO and HOMO → LUMO+1 excitations (the second and the fourth, of A symmetry and almost dark for OPA). The four orbitals arise in turn from the weak interaction of the two HOMO's and two LUMO's of the two naphthol moieties (e.g., a and b). Assuming a localized picture, these four states of the dimer arise from the two bright local (L) excitations HOMOa → LUMOa and HOMOb → LUMOb and from the two dark CT states HOMOa → LUMOb and HOMOb → LUMOa. Taking their symmetric L_+ (an excitonic state) and CT_+ and antisymmetric L_- and CT_- combinations, it is easy to see that just one of these four states carries an oscillator strength (L_+) and that they can mostly interact in couples (L_+ and CT_+, L_- and CT_-), giving rise to two partially bright states (the first and the third) and two dark states (the second and the fourth).[82] Deviation from this idealized situation is due to partial coupling with other states, besides the fact that we are in reality dealing with not fully symmetric localized states. In this picture, the stronger OPA absorber is the one that is most similar to L_+, whereas the weaker absorber is closer to CT_+. This analysis yields a possible explanation for the differences between CAM-B3LYP (L_+ more stable) and B3LYP results (CT_+ more stable) since it is well-known that B3LYP overestimates the stability of CT states. It is therefore possible to highlight a further challenge in the treatment of R-BINOL that arise from the possible couplings of excitonic and CT states, whose reliable description must be carefully checked in TD-DFT calculations.

The application of the same qualitative arguments adopted for the first four states is much more troublesome for the cluster of highly excited states at 5.2−5.6 eV, due to the strong mixing and the high number of contributing excitations. In this sense, in systems like R-BINOL the comparison of standard hybrid (like B3LYP) and recent functional developed to better treat CT states is highly recommended and, in our specific example, the fact that the two functionals yield qualitatively similar results in the condensed phase is an important finding that supports the reliability of our results.

Quite recently, a study of the performance of a choice of exchange−correlation density functionals, including both B3LYP and CAM-B3LYP, in computing local, Rydberg, and intramolecular CT excitation energies was performed.[40] In this study, the authors analyzed the correlation between the error in the computed excitation energies and the spatial overlap between occupied and virtual orbitals, through a quantity, the Λ overlap, defined in ref 40. The authors observed that there is virtually no correlation between excitation errors and Λ overlap for CAM-B3LYP, which is the recommended functional for excitation energy calculations, and the one that has a balanced description of local, Rydberg, and CT excitations. For B3LYP, the authors see a clear correlation between Λ overlap values and errors in excitation energies, with errors increasing as Λ decreases. In what the authors define as a Λ diagnostic test, values of the Λ overlap lower than 0.3 are associated, for B3LYP, with significant, in some cases on the order of a few electronvolts, errors in the excitation energies. Table A4 in the Supporting Information shows the results of the Λ diagnostic test for the lowest 30 excited states of BINOL computed in THF with both B3LYP and CAM-B3LYP. The lowest value of Λ for B3LYP is greater than 0.58 (10th excited state), indicating, according to the conclusions of ref 40, errors in excitation energies within 1 eV, and a rather

satisfactory description of the excited states of CT character. Similar values of Λ are obtained for CAM-B3LYP, where, however, as mentioned before, there is no reason to expect deviations greater than a fraction of an electronvolt independent of the results of the Λ diagnostic test.

4. CONCLUSIONS

In this paper we discussed in detail the computational studies carried out on the linear and nonlinear absorption and dichroism spectra of R-BINOL, making a special emphasis on the latter, and in particular, on the TPCD measured recently in our group. This analysis therefore followed and completed the account of the study presented in refs 16, 18, and 19, yielding a deeper insight into the computational challenges for the simulation and interpretation of one- and two-photon chiroptical properties in systems exhibiting structural chirality and which are attracting increasing interest in modern chemical research.[20,7] The calculations were carried out employing TD-DFT[33,34] with Dunning's correlation consistent aug-cc-pVDZ basis set,[59] simulating the response of both the isolated molecule and that of molecules solvated in THF. For the latter, which reproduced the conditions of the experiment, a PCM[45−49] was adopted. The TD-DFT calculations included 30 excited electronic states in the isolated molecule studies, this number reducing to 25 for the condensed-phase simulations. Magnetic gauge origin independent approaches were employed for the CD calculations.

R-BINOL is a prototype of systems exhibiting chirality induced by secondary structure. Its size and the large delocalization of the electronic density implies a relatively large number of excited electronic states lying in the region of energy probed by experimentalists in both linear and nonlinear spectroscopies, a region that is extended to reach and go below wavelengths of 200 nm. For systems as R-BINOL, TD-DFT is nowadays the only reliable computational approach available to computational chemists, and yet for several aspects computational chemistry finds itself facing some quite formidable challenges.

The energies and properties of the excited states exhibited a strong dependence on the functional and on the solvent; in our study we have compared results obtained with the widely employed B3LYP[35−37] functional and those yielded by its long-range corrected version, the increasing popular CAM-B3LYP functional,[38,39] developed especially to account for long-range dispersion and CT excitations. We showed that, when the effect of the solvent is properly taken into account (and PCM performs satisfactorily for this purpose) both functionals yielded reasonable predictions for both linear (OPA, ECD) and nonlinear (TPA, TPCD) spectroscopic properties. Focusing on CD, B3LYP was in the best agreement with experiment[75] for ECD, especially from the point of view of the intensity; CAM-B3LYP on the other hand reproduced some of the fine details at the blue edge of the experimental spectrum while overestimating apparently the strength of the linear CD signal. Looking at the TPCD spectrum, neglecting the striking differences in intensities between theory and experiment,[16,18,19] B3LYP reproduced well some of the details (the relative intensity of the two peaks apparently lying below the broad experimental band with maximum at about 240 nm) and fared better on the location of the peaks. CAM-B3LYP, on the other hand, overestimated as usual the excitation energies and therefore yielded a spectrum that is blue-shifted by ca. 30 nm, but it reproduced excellently the distance between the two major peaks and their relative intensity. Furthermore, this functional was able to predict better the shape of the spectrum at the blue edge of the spectrum. In all cases, extending the TD-DFT calculations to at least 25 excited states was found to be imperative to cover the range of wavelengths of interest in experiment. This means large, computational intensive calculations, where a tight control of the technical details (thresholds) of the calculations became mandatory. Also, the higher lying excited states did not mix with ionic states.[78,79] We have shown that B3LYP higher lying excited states are within 0.3−0.4 eV from the ionization limit, whereas CAM-B3LYP excited states rested a more comfortable 0.6−0.8 eV away from the same limit. For all these challenging aspects of the calculation of linear and nonlinear optical properties of molecules as BINOL, exhibiting structural chirality and therefore quite large and with a large density of excited states within the region of frequencies of experimental interest, promising future developments are expected from the ongoing work in the field of Kohn−Sham linear scaling[83] complex[84] or damped[85] response theory.

At least in the high energy range of the spectra, the high density of electronic states together with the high sensitivity of their properties to small perturbations (as those represented by a solvent of intermediate polarity, or slight changes in the level of theory) strongly suggest the existence of remarkable vibronic couplings. In fact, an extended analysis of the main excitations shows that, beyond a given threshold in the energy, no one-to-one correspondence of the excited states obtained at different computational levels can safely be established. This demonstrates the strength of the coupling, related to the high density of states in a small energy window. With such a scenario, a proper description of the interactions of vibrational and electronic states would be very helpful, since they were already proven to strongly modulate the electronic response in linear[86−89,41,42] and nonlinear CD spectra[43] of systems even simpler than R-BINOL, and where the lower density of states permitted a perturbative approach (Herzberg−Teller like) to the vibronic problem. Given the high density of states in R-BINOL, a full variational vibronic approach, out of reach at the state-of-the-art, would be necessary.

The pair structure of the electronic states, due to the weak coupling of the two naphthol moieties, suggests the possibility of strong mixing of CT and local exciton states, something seen in several similar cases in DNA oligomers.[69,70] Our orbital analysis gives good evidence of this occurrence. This proves to be a challenge for current density functionals. The apparent good performance of B3LYP might be related to the use of symmetric configurations. Fluctuations in the geometry, involving even tiny distortions of the molecule, yielding structures with a net charge redistribution between the two moieties, with net negative and positive excess charges on the two naphthol units, are unaccounted for in our study, and they might change the picture.

In this study we noted that one-photon response is in most cases stronger in solvent than in the gas phase. This evidence might be a spurious effect of the standard linear-response implementation of PCM[90] within the framework of the TD-DFT description of solvent effects on excited states.[91] State-specific implementations have been proposed[92,93] but, at the state of the art, they are only available for one-photon properties and, being based on iterative-solutions, their application is computationally demanding and unfeasible for the whole set of states investigated in the present contribution. In our view, a critical comparison of the linear-response and state-specific predictions of the solvent effect on nonlinear properties in the

framework of TD-DFT approach and continuum solvent models, is one of the challenges to face in the next future.

The final comment is left to the analysis of the disagreement existing between theory and experiment on the intensity of the TPA and, far more strikingly, the TPCD signal. The shortcomings of our approximations for the calculation of TPCD spectra have been discussed at length in our previous papers on the subject, see in particular refs 13−15 and 44. Electron correlation and basis set requirements, the effect of solvent and conformational variety, the choice of the functional, and the influence of molecular vibrations[43] have been discussed thoroughly. In the case of R-BINOL we have analyzed, in particular, the effect of the slow scissoring motion of the two naphthols and found that it is highly unlikely that an accurate account of the effect of this vibrational mode might influence the computed TPCD intensity, let alone recover a factor of 350, as observed. Small changes of geometry on the reference structure are also found to yield negligible changes on both the form and the overall intensity of the spectra. Also, an in depth analysis of the molecular orbitals and the structure of the excitation manifold leads to the prediction of likely coupling of CT and localized excitonic transitions in R-BINOL. Since the coupling involves states that are quite high in energy (and, by necessity, clustered in a narrow energy interval), it is not easy to estimate how large its effect on the intensity can be. In short, it is difficult, with our current knowledge, to imagine a mechanism that might explain both the large discrepancy in intensity for the nonlinear absorption and dichroism response, and the excellent agreement observed for the linear spectroscopies, going along with the rather satisfactory agreement that can be claimed on the major features of the lineshapes of TPA and TPCD spectra. It is therefore reasonable to conclude that, at this stage, there is no evidence that a theoretical or a computational explanation for the huge discrepancy might be found.

■ ASSOCIATED CONTENT

Supporting Information. Discussion of the theoretical background. Table of structural parameters. Table of excitation energies and wavelengths, TPCD parameters and rotatory strengths, TPA parameters and transition probability, ECD rotatory strength, and OPA oscillator strength. Table of the analysis of the excited electronic states of R-BINOL. Table of Λ values. Figures of C_0 and C_1 structures and Kohn−Sham orbitals. This information is available free of charge via the Internet at http://pubs.acs.org.

■ AUTHOR INFORMATION

Corresponding Author

*E-mail: rizzo@ipcf.cnr.it.

Present Addresses

▽Formerly at IPCF-CNR, Pisa, Italy.

■ ACKNOWLEDGMENT

This work is supported by the National Nature Science Foundation of China (Grant No. 21003085) and Independent Innovation Foundation of Shandong University (2009HW002), by the Swedish Research Council (VR), by the Norwegian Supercomputing Program, by the network Village (http://village.ipcf.cnr.it) and by the Italian IIT (Project Seed HELYOS).

■ REFERENCES

(1) Nakanishi, K.; Berova, N.; Woody, R. W. *Circular dichroism: principles and applications*; VCH Publishers Inc.: New York., 1994.

(2) Barron, L. D. *Molecular Light Scattering and Optical Activity*; Cambridge University Press: Cambridge, U.K., 2004.

(3) Condon, E. U. *Rev. Mod. Phys.* **1937**, *9*, 432–457.

(4) Caldwell, D. J.; Eyring, H. *The theory of optical activity*; Wiley-Interscience: New York, 1971.

(5) Moscowitz, A. In *Optical Rotatory Dispersion*; Djerassi, C., Ed.; McGraw-Hill: New York, 1960.

(6) First principle symmetry forbidden electric dipole one-photon transitions appear in rather unusual chiral point groups, i.e., C_n ($n > 3$), D_n, T, O, or I.

(7) Rivera-Fuentes, P.; Alonso-Gómez, J. L.; Petrovic, A. G.; Sailer, P.; Santoro, F.; Harada, N.; Berova, N.; Rzepa, H. S.; Diederich, F. *Chem.—Eur. J.* **2010**, *16*, 9796–9807.

(8) Tinoco, I., Jr. *J. Chem. Phys.* **1975**, *62*, 1006–1009.

(9) Denk, W.; Svoboda, K. *Neuron.* **1997**, *18*, 351–357.

(10) Power, E. A. *J. Chem. Phys.* **1975**, *63*, 1348–1350.

(11) Jansík, B.; Rizzo, A.; Ågren, H. *Chem. Phys. Lett.* **2005**, *414*, 461–467.

(12) Rizzo, A.; Jansík, B.; Pedersen, T. B.; Ågren, H. *J. Chem. Phys.* **2006**, *125*, 064113-1–064113-11.

(13) Jansík, B.; Rizzo, A.; Ågren, H. *J. Phys. Chem. B* **2007**, *111*, 446–460. Jansík, B.; Rizzo, A.; Ågren, H. Erratum. *J. Phys. Chem. B* **2007**, *111*, 2409–2414.

(14) Jansík, B.; Rizzo, A.; Ågren, H.; Champagne, B. *J. Chem. Theory Comput.* **2008**, *4*, 457–467.

(15) Rizzo, A.; Lin, N.; Ruud, K. *J. Chem. Phys.* **2008**, *128*, 164312-1–164312-17.

(16) De Boni, L.; Toro, C.; Hernández, F. E. *Opt. Lett.* **2008**, *33*, 2958–2960.

(17) Wanapun, D.; Wampler, R. D.; Begue, N. J.; Simpson, G. J. *Chem. Phys. Lett.* **2008**, *455*, 6–12.

(18) Toro, C.; De Boni, L.; Lin, N.; Santoro, F.; Rizzo, A.; Hernández, F. E. *Chem.—Eur. J.* **2010**, *16*, 3504–3509.

(19) Toro, C.; De Boni, L.; Lin, N.; Santoro, F.; Rizzo, A.; Hernández, F. E. *Chirality* **2010**, *22*, E-202–210.

(20) Rivera-Fuentes, P.; Alonso-Gómez, J. L.; Petrovic, A. G.; Santoro, F.; Harada, N.; Berova, N.; Diederich, F. *Angew. Chem., Int. Ed.* **2010**, *49*, 2247–2250.

(21) Nafie, L. A.; Keiderling, T. A.; Stephens, P. J. *J. Am. Chem. Soc.* **1976**, *98*, 2715–2723.

(22) Hecht, L.; Barron, L. D. In *Modern Aspects of Raman Spectroscopy*; Laserna, J. J., Ed.; Wiley: New York, 1996; pp 265−304.

(23) Setnička, V.; Urbanová, M.; Bouř, P.; Král, V.; Volka, K. *J. Phys. Chem A* **2001**, *105*, 8931–8938.

(24) Nakao, K.; Kyogoku, Y.; Sugeta, H. *Faraday Discuss.* **1994**, *99*, 77–85.

(25) Liégeois, V. *ChemPhysChem* **2009**, *10*, 2017–2025.

(26) Di Bari, L.; Pescitelli, G.; Salvadori, P. *J. Am. Chem. Soc.* **1999**, *121*, 7998–8004.

(27) Mason, S. F.; Seal, R. H.; Roberts, D. R. *Tetrahedron* **1974**, *30*, 1671–1682.

(28) Di Bari, L.; Pescitelli, G.; Marchetti, F.; Salvadori, P. *J. Am. Chem. Soc.* **2000**, *122*, 6395–6398.

(29) Rosini, C.; Superchi, S.; Peerlings, H. W. I.; Meijer, E. W. *Eur. J. Org. Chem.* **2000**, *1*, 61–71.

(30) Tinoco, I., Jr. *Adv. Chem. Phys.* **1962**, *4*, 113–160.

(31) Harada, N.; Nakanishi, K. *Circular Dichroic Spectroscopy − Exciton Coupling in Organic Stereochemistry*; University Science Books: Mill Valley, CA, 1983.

(32) Berova, N.; Nakanishi, K. In *Circular Dichroism: Principles and Applications*, 2nd ed.; Berova, N., Nakanishi, K., Woody, R. W., Eds.; Wiley-VCH: New York, 2000; pp 337−382.

(33) Runge, E.; Gross, E. K. U. *Phys. Rev. Lett.* **1984**, *52*, 997–1000.

(34) Marques, M. A. L.; Gross, E. K. U. *Annu. Rev. Phys. Chem.* **2004**, *55*, 427–455.
(35) Becke, A. D. *J. Chem. Phys.* **1993**, *98*, 5648–5652.
(36) Becke, A. D. *Phys. Rev. A* **1988**, *38*, 3098–3100.
(37) Lee, C.; Yang, W.; Parr, R. G. *Phys. Rev. B* **1988**, *37*, 785–789.
(38) Yanai, Y.; Tew, D. P.; Handy, N. C. *Chem. Phys. Lett.* **2004**, *393*, 51–57.
(39) Peach, M. J. G.; Helgaker, T.; Sałek, P.; Keal, T. W.; Lutnæs, O. B.; Tozer, D. J.; Handy, N. C. *Phys. Chem. Chem. Phys.* **2006**, *8*, 558–562.
(40) Peach, M. J. G.; Benfield, P.; Helgaker, T.; Tozer, D. J. *J. Chem. Phys.* **2008**, *128*, 044118-1–044118-8.
(41) Lin, N.; Luo, Y.; Santoro, F.; Zhao, X.; Rizzo, A. *Chem. Phys. Lett.* **2008**, *464*, 144–149.
(42) Lin, N.; Santoro, F.; Zhao, X.; Rizzo, A.; Barone, V. *J. Phys. Chem. A* **2008**, *112*, 12401–12411.
(43) Lin, N.; Santoro, F.; Rizzo, A.; Luo, Y.; Zhao, X.; Barone, V. *J. Phys. Chem. A* **2009**, *113*, 4198–4207.
(44) Guillaume, M.; Ruud, K.; Rizzo, A.; Monti, S.; Lin, Z.; Xu, X. *J. Phys. Chem. B* **2010**, *114*, 6500–6512.
(45) Miertuš, S.; Scrocco, E.; Tomasi, J. *Chem. Phys.* **1981**, *55*, 117–129.
(46) Tomasi, J.; Persico, M. *Chem. Rev.* **1994**, *94*, 2027–2094.
(47) Cammi, R.; Tomasi, J. *J. Comput. Chem.* **1995**, *16*, 1449–1458.
(48) Cammi, R.; Cossi, M.; Mennucci, B.; Tomasi, J. *J. Chem. Phys.* **1996**, *105*, 10556–10564.
(49) Tomasi, J.; Mennucci, B.; Cammi, R. *Chem. Rev.* **2005**, *105*, 2999–3093.
(50) Johnsen, M.; Ogilby, P. R. *J. Phys. Chem. A* **2008**, *112*, 7831–7839.
(51) Gao, J. *Acc. Chem. Res.* **1996**, *29*, 298–305.
(52) Paterson, M. J.; Kongsted, J.; Christiansen, O.; Mikkelsen, K. V.; Nielsen, C. B. *J. Chem. Phys.* **2006**, *125*, 184501-1–184501-14.
(53) Poulsen, T. D.; Ogilby, P. R.; Mikkelsen, K. V. *J. Chem. Phys.* **2001**, *115*, 7843–7851.
(54) Sahnoun, R.; Koseki, S.; Fujimura, Y. *J. Mol. Struct.* **2005**, *735*−*736*, 315–324.
(55) Krishnan, R.; Binkley, J.; Seeger, R.; Pople, J. *J. Chem. Phys.* **1980**, *72*, 650–654.
(56) Blaudeau, J.-P.; McGrath, M. P.; Curtiss, L. A.; Radom, L. *J. Chem. Phys.* **1997**, *107*, 5016–5021.
(57) Clark, T.; Chandrasekhar, J.; Schleyer, P. v. R. *J. Comput. Chem.* **1983**, *4*, 294–301.
(58) Polavarapu, P. Personal communication.
(59) Dunning, T. H., Jr. *J. Chem. Phys.* **1989**, *90*, 1007–1023.
(60) Barone, V.; Cossi, M.; Tomasi, J. *J. Chem. Phys.* **1997**, *107*, 3210–3221.
(61) Mikkelsen, K. V.; Cesar, A.; Ågren, H.; Jensen, H. J. Aa. *J. Chem. Phys.* **1995**, *103*, 9010–9023.
(62) Cammi, R.; Frediani, L.; Mennucci, B.; Tomasi, J.; Ruud, K.; Mikkelsen, K. V. *J. Chem. Phys.* **2002**, *117*, 13–26.
(63) Cammi, R.; Frediani, L.; Mennucci, B.; Ruud, K. *J. Chem. Phys.* **2003**, *119*, 5818–5827.
(64) London, F. *J. Phys. Radium* **1937**, *8*, 397–409.
(65) Bak, K. L.; Hansen, Aa. E.; Ruud, K.; Helgaker, T.; Olsen, J.; Jørgensen, P. *Theor. Chim. Acta* **1995**, *90*, 441–458.
(66) Pecul, M.; Ruud, K.; Helgaker, T. *Chem. Phys. Lett.* **2004**, *388*, 110–119.
(67) DALTON, a molecular electronic structure program, 2005, Release 2.0, see http://www.kjemi.uio.no/software/dalton/dalton.html.
(68) Frisch, M. J.; Trucks, G. W.; Schlegel, H. B.; Scuseria, G. E.; Robb, M. A.; Cheeseman, J. R.; Montgomery, J. A., Jr.; Vreven, T.; Kudin, K. N.; Burant, J. C.; Millam, J. M.; Iyengar, S. S.; Tomasi, J.; Barone, V.; Mennucci, B.; Cossi, M.; Scalmani, G.; Rega, N.; Petersson, G. A.; Nakatsuji, H.; Hada, M.; Ehara, M.; Toyota, K.; Fukuda, R.; Hasegawa, J.; Ishida, M.; Nakajima, T.; Honda, Y.; Kitao, O.; Nakai, H.; Klene, M.; Li, X.; Knox, J. E.; Hratchian, H. P.; Cross, J. B.; Bakken, V.; Adamo, C.; Jaramillo, J.; Gomperts, R.; Stratmann, R. E.; Yazyev, O.; Austin, A. J.; Cammi, R.; Pomelli, C.; Ochterski, J. W.; Ayala, P. Y.; Morokuma, K.; Voth, G. A.; Salvador, P.; Dannenberg, J. J.; Zakrzewski, V. G.; Dapprich, S.; Daniels, A. D.; Strain, M. C.; Farkas, O.; Malick, D. K.; Rabuck, A. D.; Raghavachari, K.; Foresman, J. B.; Ortiz, J. V.; Cui, Q.; Baboul, A. G.; Clifford, S.; Cioslowski, J.; Stefanov, B. B.; Liu, G.; Liashenko, A.; Piskorz, P.; Komaromi, I.; Martin, R. L.; Fox, D. J.; Keith, T.; Al-Laham, M. A.; Peng, C. Y.; Nanayakkara, A.; Challacombe, M.; Gill, P. M. W.; Johnson, B.; Chen, W.; Wong, M. W.; Gonzalez, C.; Pople, J. A. *Gaussian 03*, Revision D.01; Gaussian, Inc.: Wallingford, CT, 2004.
(69) Santoro, F.; Barone, V.; Improta, R. *Proc. Natl. Acad. Sci. U.S.A.* **2007**, *104*, 9931–9936.
(70) Santoro, F.; Barone, V.; Improta, R. *J. Am. Chem. Soc.* **2009**, *131*, 15232–15245.
(71) Crespo-Hernández, C. E.; Cohen, B.; Hare, P. M.; Kohler, B. *Chem. Rev.* **2004**, *104*, 1977–2019.
(72) Takaya, T.; Su, C.; de La Harpe, K.; Crespo-Hernández, C. *Proc. Natl. Acad. Sci. U.S.A.* **2008**, *105*, 10285–10290.
(73) Ziegler, T.; Krykunov, M. *J. Chem. Phys.* **2010**, *133*, 074104-1–074104-11.
(74) Fischer, P.; Wise, F. W.; Albrecht, A. C. *J. Phys. Chem. A* **2003**, *107*, 8232–8238.
(75) Kriech, M. A.; Conboy, J. C. *Appl. Spectrosc.* **2005**, *59*, 746–753.
(76) Jacquemin, D.; Wathelet, V.; Perpéte, E. A.; Adamo, C. *J. Chem. Theor. Comput.* **2009**, *5*, 2420–2435.
(77) Santoro, F.; Barone, V.; Improta, R. *J. Comput. Chem.* **2008**, *29*, 957–964.
(78) Casida, M. E.; Jamorski, C.; Casida, K. C.; Salahub, D. R. *J. Chem. Phys.* **1998**, *108*, 4439–4449.
(79) Lehtonen, O.; Sundholm, D.; Send, R.; Johansson, M. P. *J. Chem. Phys.* **2009**, *131*, 024301-1–024301-13.
(80) Monshouwer, R.; Abrahamsson, M.; van Mourik, F.; van Grondelle, R. *J. Phys. Chem. B* **1997**, *101*, 7241–7248.
(81) Plotner, J.; Tozer, D. J.; Dew, A. *J. Chem. Theory Comput.* **2010**, *6*, 2315–2324.
(82) Improta, R.; Santoro, F.; Barone, V.; Lami, A. *J. Phys. Chem. A* **2009**, *113*, 15346–13354.
(83) Kjærgaard, T.; Jørgensen, P.; Olsen, J.; Coriani, S.; Helgaker, T. *J. Chem. Phys.* **2008**, *129*, 054106-1–054106-23.
(84) Norman, P.; Bishop, D. M.; Jensen, H. J. Aa.; Oddershede, J. *J. Chem. Phys.* **2005**, *123*, 194103-1–194103-18.
(85) Kristensen, K.; Kauczor, J.; Kjærgaard, T.; Jørgensen, P. *J. Chem. Phys.* **2009**, *131*, 044112-1–044112-33.
(86) Neugebauer, J.; Baerends, E. J.; Noojien, M.; Autschbach, J. *J. Chem. Phys.* **2005**, *122*, 234305-1–234305-7.
(87) Nooijen, M. *Int. J. Quantum Chem.* **2006**, *106*, 2489–2510.
(88) Dierksen, M.; Grimme, S. *J. Chem. Phys.* **2006**, *124*, 174301-1–174301-12.
(89) Bloino, J.; Biczysko, M.; Santoro, F.; Barone, V. *J. Chem. Theor. Comput.* **2010**, *6*, 1256–1274.
(90) Cossi, M.; Barone, V. *J. Chem. Phys.* **2001**, *115*, 4708–4717.
(91) Corni, S.; Cammi, R.; Mennucci, B.; Tomasi, J. *J. Chem. Phys.* **2005**, *123*, 134512-1–134512-10.
(92) Caricato, M.; Mennucci, B.; Tomasi, J.; Ingrosso, F.; Cammi, R.; Corni, S.; Scalmani, G. *J. Chem. Phys.* **2006**, *124*, 124520-1–124520-13.
(93) Improta, R.; Barone, V.; Scalmani, G.; Frisch, M. J. *J. Chem. Phys.* **2005**, *125*, 054103-1–054103-9.